Biophysical Journal, Volume *116*

Supplemental Information

Gramicidin Increases Lipid Flip-Flop in Symmetric and Asymmetric Lipid Vesicles

Milka Doktorova, Frederick A. Heberle, Drew Marquardt, Radda Rusinova, R. Lea Sanford, Thasin A. Peyear, John Katsaras, Gerald W. Feigenson, Harel Weinstein, and Olaf S. Andersen

Table S1. Asymmetric samples examined in each experiment. Shown are the donor and acceptor lipid pairs; the corresponding experiments (Exp.); gA-to-lipid ratio (gA:L); nominal donor:acceptor ratio (D:A); mole fraction of donor in the final asymmetric sample determined from GC (χ_{don}); and the area fraction of the shifted choline resonance peak measured with NMR after sample preparation ($C_{\mathrm{out}}(t=0)$) indicating the initial fraction of donor lipid on the outer leaflet of the vesicles.

Donor	Acceptor	Exp.	gA:L	D:A	χ_{don}	$C_{\mathrm{out}}(t=0)$
POPC-d31	POPC	GBFA	1:20000	2	0.32	-
	POPC-d13	SAXS	1:40	3	0.4	-
		NMR	0	2	0.34	0.87 (0.03)
			1:40	2	0.33	0.76 (0.02)
			1:100	3	0.38	0.76 (0.02)
DMPC-d54	POPC	GBFA	1:20000	2	0.35	-
		CD	1:40	3	0.45	-
		DSC	0	3	0.42	-
			1:40	3	0.4	-
	POPC-d13	NMR	0	3	0.43	0.85 (0.02)
			1:40	3	0.4	0.78 (0.01)
			1:200	3	0.42	0.88 (0.01)

Table S2. Representative vesicle sizes measured with dynamic light scattering (DLS). Shown are the acceptor and donor lipid composition, and the diameter (D) and polydispersity index (PI) of the symmetric acceptor vesicles and the final asymmetric vesicles.

acceptor	donor	symmetric acceptor LUVs		final asymmetric LUVs	
		D [nm]	PI	D [nm]	PI
POPC-d13/gA (1:40)	POPC-d31	146.6	0.072	153.9	0.123
POPC-d13/gA (1:100)		129.9	0.005	129.2	0.118
POPC-d13	DMPC-d54	122.8	0.108	126.9	0.151
POPC/gA (1:40)		137.0	0.101	136.8	0.216
POPC/gA (1:20,000)		122.5	0.109	128.0	0.131

Table S3. Effect of Pr^{3+} on bilayer properties. The rates of ANTS quenching by TI^{+} in symmetric LUVs composed of DEPC (di22:1 PC) and gA at gA:lipid ratio of 1:2096, and mixed with different amounts of the shift reagent Pr^{3+}. (In the NMR experiments described in the text the sample gets exposed to at most 0.1 mM Pr^{3+} after the three Pr^{3+} titrations, which corresponds to a Pr^{3+}:lipid ratio of ~1:7.) The ANTS quenching rates are representative of bilayer compressibility with an increase and decrease indicating softening and stiffening of the bilayer, respectively. Relative to the sample without Pr^{3+}, no significant changes in the rate were observed, confirming that the shift reagent does not alter bilayer properties.

Composition	Pr^{3+}:lipid ratio	Average Rate (s^{-1})	Stdev
gA	0	24.2	1.7
gA + 3 mM Pr^{3+}	60	21.9	2.3
gA + 10 mM Pr^{3+}	200	25.6	3.4

Table S4. Simulated bilayers without gramicidin. Shown are the total simulation time and the last equilibrated portion of each trajectory used for analysis. Equilibration was assessed from convergence of the area per lipid quantified with the algorithm from [1]. Also shown for each leaflet are the average area per lipid, A_{lip} (equal to the lateral area of the simulation box divided by the number of lipids in the leaflet); the area compressibility modulus, K_A (calculated from local thickness fluctuations as described in [2]); the bending rigidity modulus, κ_C (calculated from local splay fluctuations as described in [3, 4]); and the average leaflet thickness (calculated as described in Section S.2). Errors are shown in parentheses. The errors on A_{lip} are standard errors calculated from consecutive time blocks of length equal to the effective number of samples [1]. Errors on K_A and κ_C were calculated as described in Refs. [2] and [3, 4], respectively.

Bilayer	Leaf	Simulation time [ns]		A_{lip} [A^2]	K_A† [mN/m]	κ_C† [k_BT]	d_0† [A]
		analysis	total				
§POPC	Top	183	226	64.3 (0.2)	236 (26)	12.9 (0.5)	17.8
	Bot				186 (28)	12.4 (0.6)	17.7
§DMPC/POPC 0.75/0.25	Top	738	738	61.4 (0.1)	282 (24)	15.4 (0.6)	16.8
	Bot				244 (38)	14.8 (0.5)	16.8
§DMPC/POPC 0.10/0.90	Top	471	471	63.8 (0.1)	238 (22)	12.8 (0.6)	17.7
	Bot				188 (32)	11.7 (0.4)	17.7
Asymmetric DMPC/POPC	Top	280	445	61.4 (0.1)	286 (32)	15 (0.5)	16.8
	Bot			63.8 (0.1)	224 (26)	12.5 (0.5)	17.7

§ Bilayer systems taken from [5].

† For the symmetric bilayers, the corresponding average leaflet quantity was used in the membrane deformations analysis described in Section S3.

Table S5. Structural parameters for POPC at 25°C obtained from modeling SAXS data.

Parameter	Symbol [units]	Value	Literature value[a]
Total lipid volume	V_L [Å^3]	1249.0	1251.5[b]
Headgroup volume	V_{HL} [Å^3]	331[b]	331[b]
Area per lipid	A_L [Å^2]	63.9	63.5
Bilayer (Luzzati) thickness	D_B [Å]	39.1	39.5
Phosphate-phosphate distance	D_{HH} [Å]	35.8	37.0
Hydrocarbon thickness	$2D_C$ [Å]	28.7	29.0

[a]Ref. [6] [b]fixed parameter

Table S6. Parameters for modeling the gA transmembrane dimer and associated water in Monte Carlo simulations of small-angle scattering curves.

Parameter	Symbol [units]	Value
Volume of gA dimer and associated water	V_{gA} [Å^3]	5456
Area of gA domain	a_{cyl} [Å^2]	221
Radius of gA domain	r_{cyl} [Å]	8.4
Thickness of gA domain	t_{cyl} [Å]	24.7
Number of associated waters	N_w	10
Total number of electrons in gA domain	N_{e^-}	2118
Electron density of gA domain	ρ_{gA} [e$^-$ Å^{-3}]	0.388

Figures

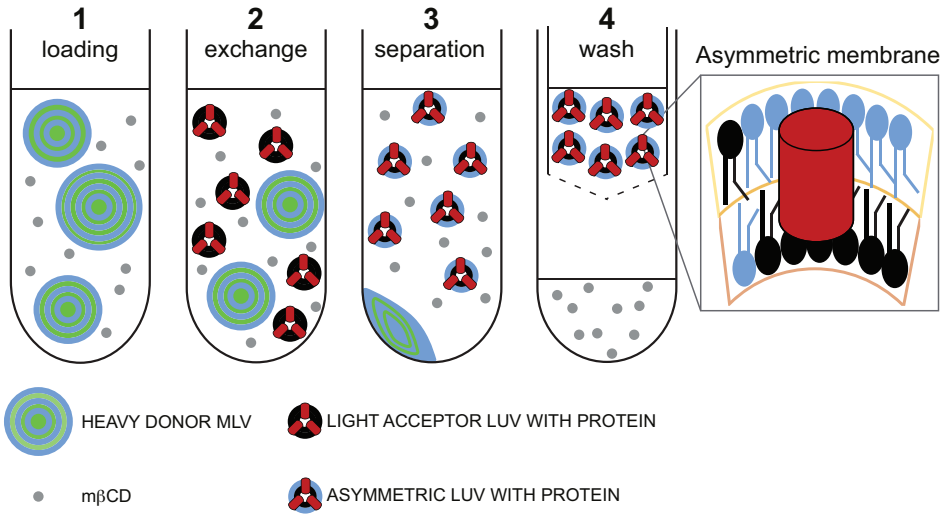

Figure S1. Schematic illustration of the protocol for preparation of asymmetric proteoliposomes. Step 1, MLVs of donor lipid are incubated with MβCD for 2 h at room temperature with gentle stirring. Step 2, extruded symmetric LUVs with gramicidin are added to the donor lipid/MβCD solution, and the acceptor/donor/MβCD mixture is incubated at room temperature with gentle stirring. Step 3, donor MLVs are separated from the asymmetric vesicles and cyclodextrin after an 8-fold dilution with H_2O and centrifugation at 20,000 x g for 30 min. Step 4, cyclodextrin is removed with centrifugal filter devices, and the sample is washed at least 3 times with water (or another appropriate solvent). The final asymmetric proteoliposomes are recovered from the retentate. The schematic is adapted from Ref. [7].

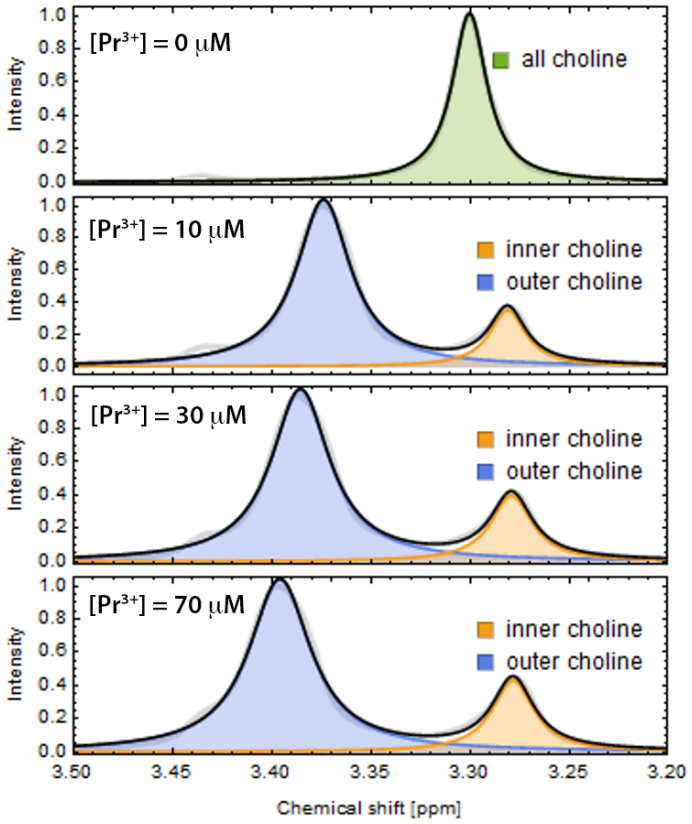

Figure S2. Representative ^{1}H NMR spectra of a gA-aLUV sample prepared with POPC-d13 acceptor and DPMC-d54 donor vesicles. In each panel, the solid gray line is the experimentally measured spectrum and the solid black line is the fitted sum of one or two Lorentzians (shown individually as shaded regions). *Upper panel*, prior to addition of the shift reagent Pr^{3+}, a single peak is observed corresponding to the headgroup-protiated donor lipid located in both leaflets. Lower three panels, external addition of increasing amounts of Pr^{3+} to the sample results in a gradual downfield shift of the outer leaflet donor lipid (blue shading). Donor lipid residing in the inner leaflet (orange shading) is essentially protected from the shift reagent. The peak areas are proportional to the amount of lipid in each environment.

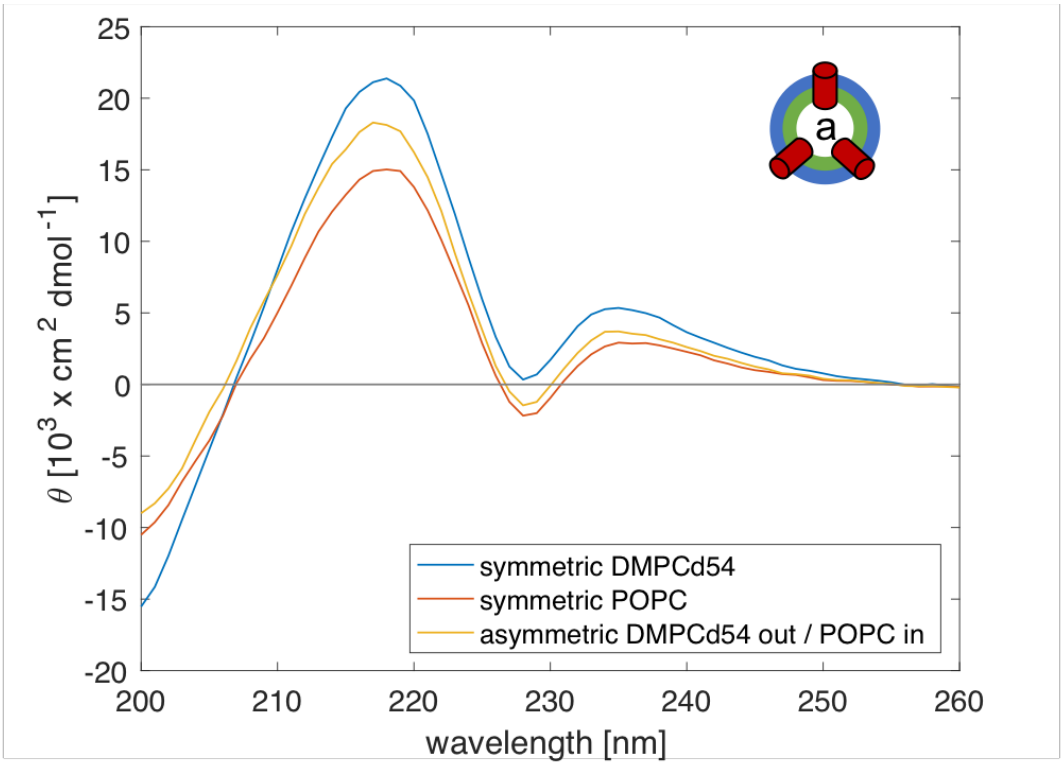

Figure S3. Circular dichroism spectra of gA-containing DMPC-d54 (blue) and POPC (red) sLUVs, and compositionally asymmetric LUVs composed of DMPC-d54 and POPC (yellow). All liposomes were prepared at a gA:lipid ratio of 1:40, and all measurements were performed at 25°C.

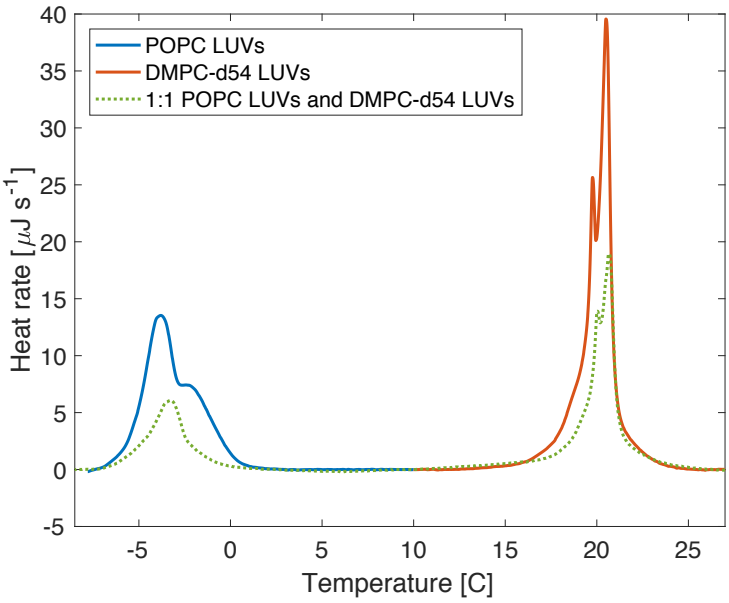

Figure S4. DSC thermograms for POPC LUVs (blue), DMPC-d54 LUVs (red) and a 1:1 mixture of POPC LUVs and DMPC-d54 LUVs (dotted green).

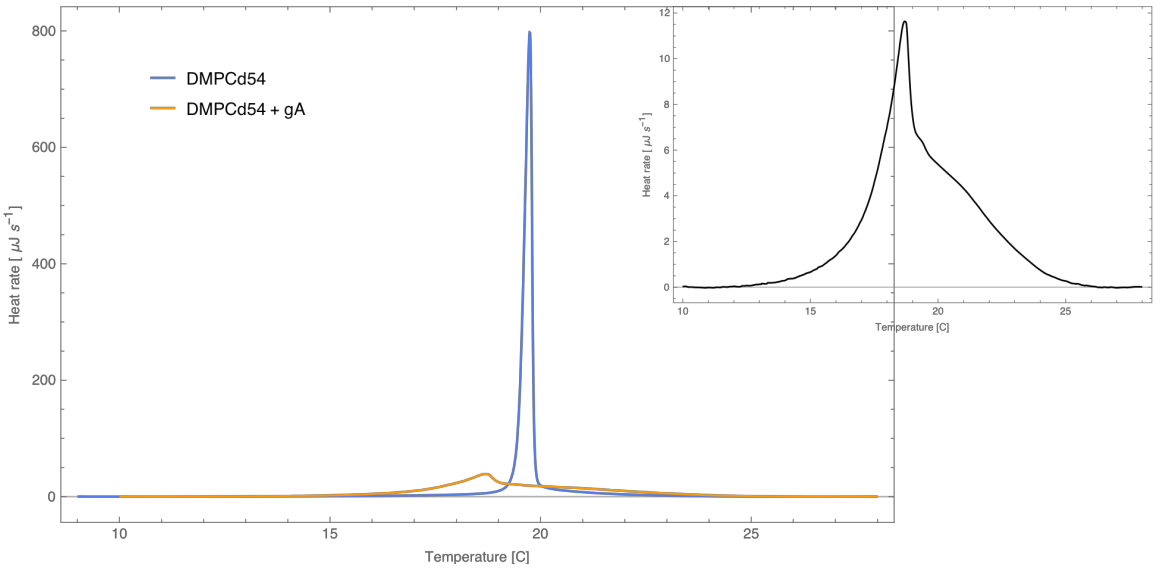

Figure S5. DSC thermograms for DMPCd54 symmetric vesicles without (blue) and with (orange) gA at gA:lipid ratio of 1:40. The inset shows a zoomed in version of the gA-sLUV thermogram. The presence of gA broadens the melting transition of the sample and slightly decreases it.

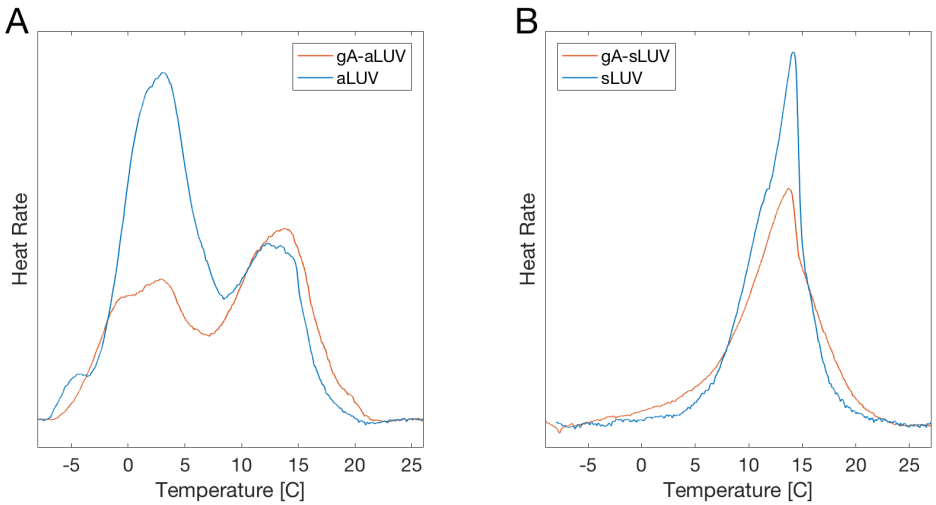

Figure S6. DSC thermograms for asymmetric (A) and symmetric vesicles (B) without and with gramicidin (at gA:lipid ratio of 1:40). The data in (A) is taken from Fig. 3 in the main text. The data in (B) is for vesicles made of DMPC-d54/POPC 75/25 mol%, a composition similar to that of the outer leaflet of the asymmetric vesicles in (A).

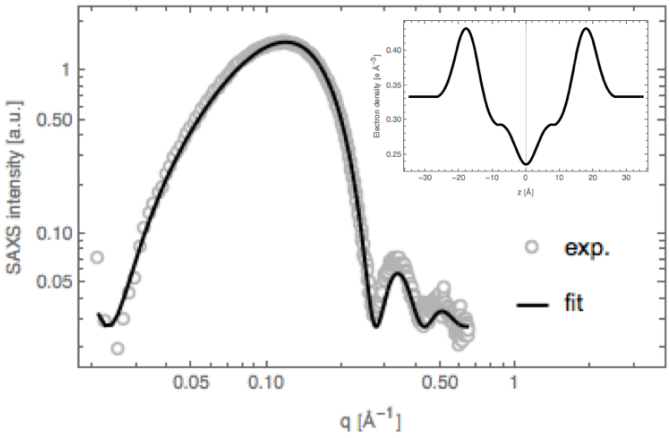

Figure S7. SAXS analysis of POPC data at 25°C. Experimental data (open circles) and fit (solid line) to a model of the lipid matter density distribution along the bilayer normal. The electron density profile corresponding to the best fit is shown in the inset.

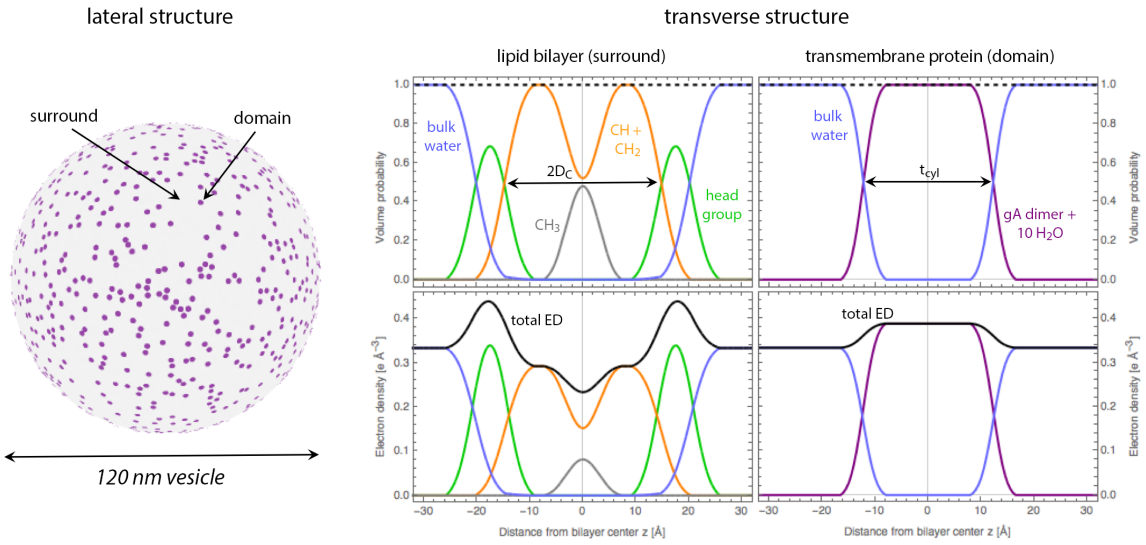

Figure S8. Schematic illustration of Monte Carlo scattering analysis. The MC analysis considers both lateral (i.e., in-plane) and transverse variation in the electron density within the proteoliposome. *Left*, the lateral structure corresponds to cylindrical gA (transmembrane dimer) domains randomly dispersed in the surrounding continuous POPC lipid bilayer. *Right*, the transverse structure of the lipid bilayer is given by the POPC volume probability profile, while that of the gA domain is given by a cylinder of uniform volume probability smoothed by convolution with a 2.0 Å-width Gaussian to mimic the effects of thermal disorder (upper panels). The corresponding total electron density (ED) profiles (black curves in lower panels) are inputs to the simulation. See Section S.4 for more details.

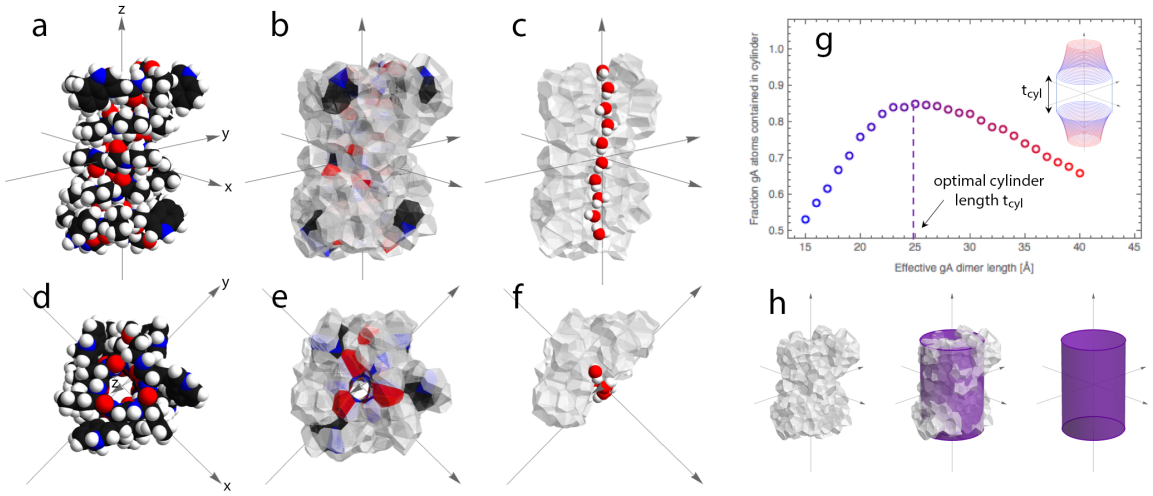

Figure S9. Determination of gramicidin channel structural parameters for Monte Carlo scattering simulations. (a) Space filling model of a gramicidin-A (gA) transmembrane dimer in a POPC bilayer from a molecular dynamics simulation, with CPK coloring (carbon is black, hydrogen is white, nitrogen is blue, oxygen is red). The z direction is normal to the (x,y) plane of the lipid bilayer. (b) A 3D Voronoi tessellation of the system yields one cell per atom, from which atomic volumes of gA and associated waters are obtained. (c) Cross-section of the 3D Voronoi representation of gA with the +x atoms removed to show the central cavity occupied by 10 water molecules (shown in space filling representation). (d), (e), and (f) are 90° rotations of panels a, b, and c, respectively, providing a view that looks down on the gA dimer from above the membrane. The water atoms are removed in panels d and e to show the central cavity. (g) Given the fixed gA+water channel volume V_{gA} obtained from the Voronoi analysis, a cylindrical representation of gA was found by maximizing the number of gA atoms enclosed in a cylinder of length t_{cyl} and area $a_{cyl} = V_{gA}/t_{cyl}$. The inset shows a graphical representation of all cylindrical volumes tested, color coded to the data points. (h) The optimal effective cylinder superimposed on the 3D Voronoi representation of gA. See Section S.4 for more details.

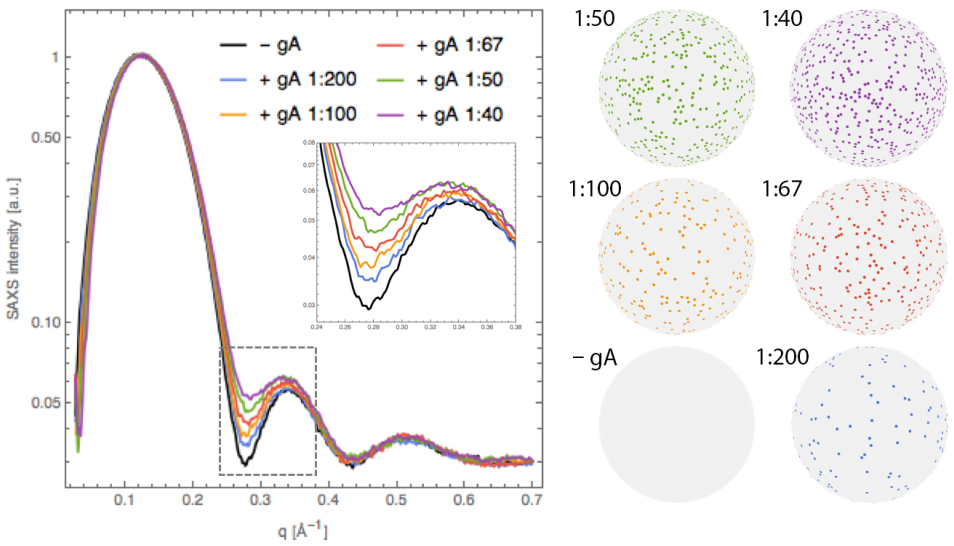

Figure S10. Effect of increasing gA concentration on simulated SAXS data. *Left*, increasing the bilayer concentration of gA up to a protein:lipid ratio of 1:40 systematically increases the intensity at the minimum between the first and second scattering lobes, shown in an expanded view in the inset. *Right*, Monte Carlo simulations snapshots corresponding to different gA:lipid ratios. See Section S.4 for more details.

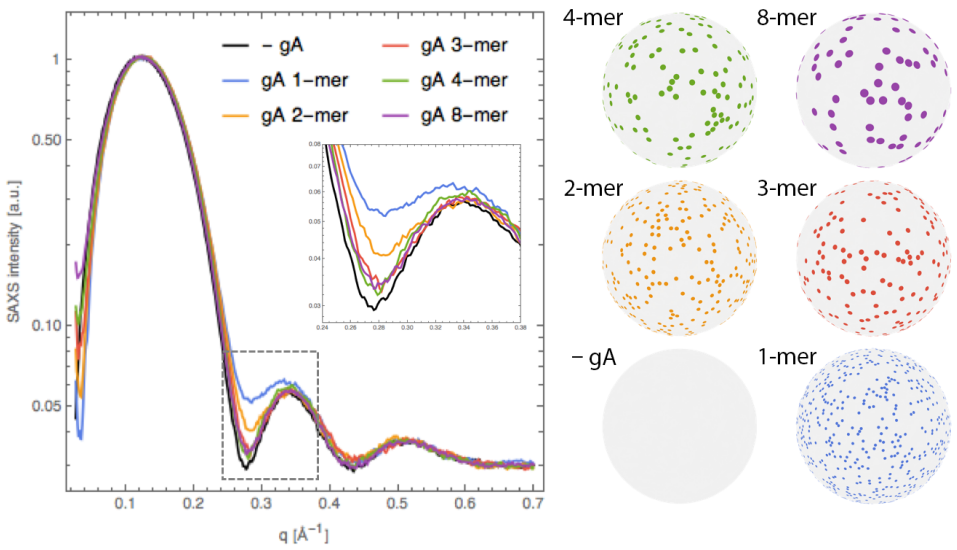

Figure S11. Effect of lateral gA association on simulated SAXS data. *Left*, lateral oligomerization of transmembrane gA dimers decreases the intensity at the minimum between the first and second scattering lobes, shown in an expanded view in the inset. A fixed gA:lipid ratio of 1:40 was used in all simulations. *Right*, Monte Carlo simulations snapshots corresponding to different oligomerization states. See Section S.4 for more details.

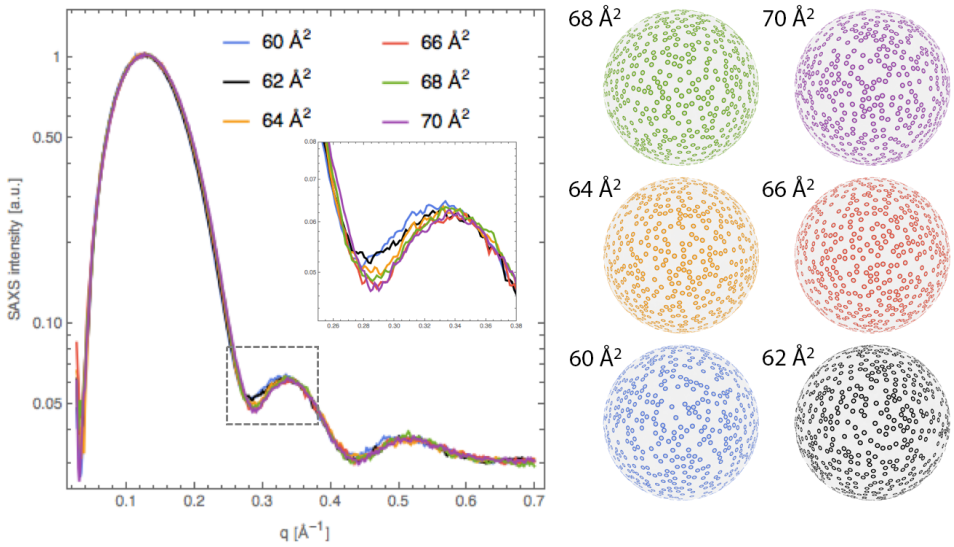

Figure S12. Effect of gA-induced lipid perturbation on simulated SAXS data. *Left*, bilayer thinning (i.e., increased area per lipid) of the first shell of 14 lipids surrounding a gA transmembrane dimer causes a slight decrease in the intensity at the minimum between the first and second scattering lobes, and a slight shift of the minimum to higher q, as shown in an expanded view in the inset. A fixed gA:lipid ratio of 1:40 and a bulk (unperturbed) area per lipid of 62.0 Å^2 were used in all simulations. *Right*, Monte Carlo simulations snapshots showing the first lipid shell surrounding the protein in a color that corresponds to the SAXS curves on the left. See Section S.4 for more details.

S.1. Simulation details. Table S4 lists all simulated bilayer systems without gramicidin. As indicated, the symmetric bilayers were taken from [5]. The asymmetric bilayer was simulated with the same simulation parameters as the symmetric ones: a 10-12 Å cutoff with NAMD's *vdwForceSwitchng* option turned on for Van der Waals and electrostatic interactions; Particle Mesh Ewald for long-range electrostatics, with grid spacing of 1 Å; Langevin thermostat set to maintain temperature at 25°C and a Nose-Hoover barostat with Langevin dynamics set to maintain pressure at 1 atm with a period of 200 fs and delay of 50 fs; and a time-step of 2 fs with fixed hydrogen bonds (i.e. *rigidbonds* option set to *all*).

The two gA-containing bilayer systems (one gA channel embedded into the symmetric POPC or asymmetric DMPC/POPC membrane as described in the text) were simulated with the same simulation parameters as outlined above.

S.2. Analysis of leaflet thickness from MD simulations. Local leaflet thicknesses were calculated with a modified version of VMD's MEMBPLUGIN tool for membrane thickness [8] as described in [2]. Briefly, the heights h of all heavy atoms on the lipid acyl chains, including the phosphate, were calculated at different grid points on the leaflet surface by interpolation on their z coordinates as follows:

$$h_{\varsigma,(x,y)} = \frac{\sum_i \frac{z_{\varsigma,i}}{d_{i,(x,y)}^2}}{\sum_i \frac{1}{d_{i,(x,y)}^2}}, \tag{S1}$$

where ς denotes the atom type (e.g. phosphate, C1 atom on the sn-1 chain, C2 atom on the sn-2 chain, etc.), x and y are the two-dimensional coordinates of the grid point, the summations are over all lipid atoms of type ς in the leaflet with $z_{\varsigma,i}$ being the z-coordinate of atom i and $d_{i,(x,y)}$ denoting the 2D distance between atom i and the grid point at (x, y). Once all heights have been calculated, the leaflet thickness τ at each grid point was simply the distance between the local height of the phosphate atom and the local height of the lowest-situated atom type at the grid point:

$$\tau_{P,(x,y)} = h_{P,(x,y)} - \min h_{(x,y)}. \tag{S2}$$

The average leaflet thickness d_0 in Table S4 is the space- and time-averaged local thickness τ_P in the leaflet.

S.3 Analysis of membrane deformation. The membrane deformation profile around a single gA channel was calculated by combining information from the simulation trajectories with the CTMD formalism in which the free energy of membrane deformation ΔG_{def} is expressed in terms of the area compressibility (K_A) and bending rigidity (κ_C) moduli of the lipid environment:

$$\Delta G_{\text{def}} = \frac{1}{2}\int_{\Omega} \left\{ K_a \left(\frac{u}{d_0}\right)^2 + \kappa_C \left(\frac{\partial^2 u}{\partial x^2} + \frac{\partial^2 u}{\partial y^2} - c_0\right)^2 - \kappa_C c_0^2 \right\} d\Omega. \tag{S3}$$

In the space integral in Eq. S3, $u = d - d_0$ is deviation from the equilibrium thickness and c_0 is spontaneous curvature. Generally, ΔG_{def} is calculated directly for the whole membrane and

used to obtain the optimal membrane deformation profile, i.e. the optimal u that minimizes ΔG_{def} subject to a number of boundary conditions.

Because the two membrane leaflets may deform in a different way around gA (especially in the case of an asymmetric membrane), here we treat each leaflet separately. Thus, if L denotes one leaflet (top or bottom) and $\Delta G_{\text{def}}^{L}$ is the corresponding free energy, then:

$$\Delta G_{\text{def}}^{L} = \frac{1}{2}\int_{\Omega} \left\{ K_a^L \left(\frac{u}{d_0}\right)^2 + \kappa_C^L \left(\frac{\partial^2 u}{\partial x^2} + \frac{\partial^2 u}{\partial y^2} - c_0\right)^2 - \kappa_C^L c_0^2 \right\} d\Omega, \qquad \text{(S4)}$$

where all mechanical constants, u, d_0 and c_0 represent the per leaflet quantities. Eq. S4 is used to obtain an optimal deformation profile for each leaflet L (as described in detail below) and the membrane deformation profile is then the sum of the deformation profiles of the two bilayer leaflets. In the procedure, the input from the MD simulations consists of (1) the mechanical constants (K_a^L and κ_C^L) and d_0 calculated from the bilayer-only trajectories as described in Section S.2 and listed in Table S4; and (2) the leaflet thickness at the gA-lipid boundary which is calculated from the gA containing trajectories as descried below and appears as one of the boundary conditions in the energy minimization procedure.

Thus, the following protocol, inspired by the methodology in [9], was used to calculate the optimal deformation profile for a leaflet L:

1. Identify the gA-lipid boundary in the leaflet and calculate the leaflet thickness at this boundary as described in the main text.
2. Solve the following boundary value problem:

$$\kappa_C^L \nabla^4 u + \left(\frac{K_a^L}{d_0^2}\right) u = 0 \qquad \text{where} \qquad \nabla^2 = \frac{\partial^2}{\partial x^2} + \frac{\partial^2}{\partial y^2} \qquad \text{(S5)}$$

subject to the boundary conditions:

$$u|_{\Gamma_{out}} = 0 \qquad \nabla u|_{\Gamma_{out}} = 0 \qquad u|_{\Gamma_{in}} = u_0(x,y) \qquad \nabla^2 u|_{\Gamma_{in}} = v_0(x,y) \qquad \text{(S6)}$$

where Γ_{out} and Γ_{in} denote the bulk and the protein-lipid interface respectively, and u_0 and v_0 are the deviation from d_0 and the curvature at the gA-lipid boundary accordingly. Both u_0 and v_0 can be non-uniform around the protein and are thus functions of x and y. $u_0(x,y)$ is calculated directly from the gA simulations by subtracting d_0 from the corresponding leaflet thickness at (x,y), while κ_C^L and K_a^L are calculated from the bilayer-only trajectories as described in the caption of Table S4.

v_0 is obtained through a self-consistent optimization procedure that aims to globally minimize $\Delta G_{\text{def}}^{L}$ by following a slightly modified version of the approach in [9]. In short, every (x,y) point on the gA-lipid boundary is first expressed as a function of an angle θ relative to the center of gA. Then $v_0(\theta)$ is expressed as a Fourier series truncated up to 7$^{\text{th}}$ order:

$$v_0(\theta) \sim \sum_{n=0}^{7} (a_n \cos n\theta + b_n \sin n\theta) \qquad \text{(S7)}$$

and is thus parameterized by only 15 parameters (a_0 through a_7 and b_1 through b_7). The 15 parameters are first chosen at random, then optimized using a quasi-Newton method for unconstrained minimization (the *fminunc* function in MATLAB) to find the minimum $\Delta G_{\mathrm{def}}^{L}$. For each set of parameters, $\Delta G_{\mathrm{def}}^{L}$ is obtained by:
(1) calculating $v_0(\theta)$ with Eq. S7,
(2) solving Eq. S5 for u subject to the four boundary conditions in Eq. S6 (which yield a unique solution), and
(3) using the resulting deformation profile u to get $\Delta G_{\mathrm{def}}^{L}$ with Eq. S4.
Eq. S5 is solved by using the 5-point stencil method (the 5-point finite difference approximation of the Laplacian operator) in two dimensions and expressing the problem in the form $Au = b$ where A is a nonsingular matrix, b is a vector and thus the solution can be computed as $u = A\backslash b$.

S.4. Analysis of SAXS data

S.4.1. Overview

In a small-angle scattering experiment, the scattering pattern at the detector is related to spatial and temporal variation in the distribution of matter on length scales of ~ 1–100 nm. More specifically, the distribution of scattering centers—electron density (ED) and neutron scattering length density (NSLD) for X-ray and neutron radiation, respectively—within the illuminated sample volume determine the coherent scattering intensity as a function of momentum transfer vector q. In a lipid bilayer, the different chemical makeup of lipid headgroups compared to their hydrocarbon chains results in a large variation in ED in the transverse direction along the bilayer normal (here referred to as the "z" direction) which results in characteristic lobes of scattering intensity vs. q (Fig. S7). In contrast, at any given z position there is much less ED variation in the (x,y) direction parallel to the plane of the bilayer. For this special case of a laterally homogeneous bilayer, the observed intensity $I(q)$ is dominated by scattering that arises from transverse variation in electron density.[1] To a very good approximation, $I(q)$ is then mathematically related to the real-space ED profile $\rho(z)$ by a simple one-dimensional Fourier transform.

The *homogeneous bilayer approximation* described above enables the prediction of X-ray (or neutron) scattering intensity given knowledge of the lipid matter density distribution across the bilayer. Conversely (and more commonly) it enables the determination of real-space structural parameters such as area per lipid and bilayer thickness from experimental scattering data when fitted with a suitable model. Fig. S7 shows the analysis of SAXS data from POPC unilamellar vesicles at 25°C using a typical transverse matter density model with distinct layers for the lipid headgroup, the combined hydrocarbon CH_2 and CH moieties, and the terminal CH_3 groups [10]. The best-fit curve produced by the model (solid black line) faithfully reproduces the experimental data (open circles), and the best-fit

[1] For spherical bilayered vesicles such as the unilamellar liposomes used in this study, the terms *transverse* and *lateral* should be replaced with *radial* and *angular*. We nevertheless use transverse and lateral instead as these terms are far more common in the literature of lipid bilayers.

parameters (Table S5) are in excellent agreement with literature values [6], demonstrating the robustness of scattering data and analysis.

Many single-component bilayers in the fluid phase have now been analyzed within the homogeneous bilayer approximation using models of varying degree of complexity [11, 12]. However, for multicomponent mixtures that exhibit substantial in-plane variation in scattering density, the homogeneous bilayer approximation is no longer valid and can fail to reproduce features in scattering data. Here, our motivation for employing a more sophisticated model that properly accounts for lateral ED variation is the enhanced scattering intensity seen at the minimum between the first two lobes of SAXS intensity in gA-containing liposomes (Fig. 1A in the main text). This feature cannot be accounted for within the homogeneous bilayer approximation, which predicts zero coherent scattering intensity at these minima for symmetric bilayers. As we will show now (and to our knowledge, for the first time), the liftoff observed in the SAXS data is in fact a hallmark of a transmembrane protein embedded in a lipid bilayer.

S.4.2. Methodology

We have previously used two different (but essentially equivalent) approaches to modeling small-angle scattering data from laterally heterogeneous bilayers. A purely analytical solution is based on a spherical harmonic expansion of the scattering potential, which separates the scattering form factor into orthogonal terms for the radial and angular scattering length density variation [13]. A simulation approach based on Monte Carlo (MC) sampling of the real-space distribution of scattering length density yields identical results to the analytical solution for the same underlying geometrical model of the bilayer [13]. Although these methods were developed specifically for the study of lipid phase separation using small-angle neutron scattering [14], the concepts apply equally well to the case of proteins embedded in lipid bilayers, as we will now show.

As mentioned previously, the standard analysis for small-angle scattering data from lipid bilayers is to model the real-space transverse scattering length density profile (in the case of SAXS data, the ED profile). This approach is inappropriate for laterally heterogeneous bilayers as it explicitly averages the in-plane structure and thus fails to capture coherent scattering arising from non-random lipid mixing or the presence of adsorbed or inserted proteins. There are two reasons why the homogeneous bilayer approximation is not valid for our experimental system: (1) the gA transmembrane dimer has a markedly different transverse ED profile than the lipid as shown in Fig. S8, resulting in a large contrast between protein and lipid and consequently a non-negligible contribution from the lateral/angular form factor; (2) the protein inclusion may perturb the local bilayer structure, resulting in additional lateral complexity. We chose to use the MC approach rather than the purely analytical solution primarily because it is relatively easy to simulate complicated geometries (such as shells of perturbed lipid) that are beyond the capabilities of the existing analytical framework.

The MC simulations, described in detail previously for the case of coexisting lipid phases [13, 14] and summarized schematically in Fig. S8, consider two environments within a unilamellar vesicle. Here, these are the gA transmembrane domains and the continuous

lipid bilayer that surrounds them. Each of these environments has a different transverse ED profile as shown in Fig. S8. We now briefly describe the different inputs to the simulations.

Transverse structure of the lipid bilayer. The ED profile obtained from fitting the POPC data in the absence of gA (Fig. S7 inset) was used as the ED profile of the continuous lipid bilayer except where noted below.

Transverse structure of the protein domain. We modeled the transverse ED profile of a gA transmembrane dimer as follows. The molecular volume of a gA dimer embedded in a POPC bilayer was determined from a 3D Voronoi tessellation of a single frame of an MD simulation as shown in Fig. S9. The Voronoi tessellation divides all atoms in the simulation box into individual 3D cells, from which effective atomic volumes are easily calculated. The total gA transmembrane dimer volume V_{gA} was calculated as the sum of the individual volumes of all atomic cells of the gA dimer, along with those of the ten water atoms lining the central cavity (Fig. S9*a-f*). An equivalent cylinder of identical volume was found by optimizing the length t_{cyl} and area a_{cyl} (where $V_{gA} = V_{cyl} = t_{cyl}a_{cyl}$) such that the resulting cylinder enclosed the largest fraction of gA atoms (Fig. S9*h*); the optimal cylinder (shown graphically in Fig. S9*g*) had a length of 24.7 Å and an area of 221 Å^2. The electron density ρ_{GA} of the gA domain was calculated as the total number of electrons in all atoms of the gA dimer and ten central waters, N_e–, divided by the gA volume V_{gA}, i.e. $\rho_{gA} = N_e-/V_{gA}$. The step ED profile is given by

$$\rho(z) = \begin{cases} \rho_{gA} & -t_{cyl}/2 < z < t_{cyl}/2 \\ \rho_w & z \le -t_{cyl}/2 \ \ or \ \ z \ge t_{cyl}/2 \end{cases}, \qquad (S1)$$

where ρ_w is the electron density of water. To account for the smoothing effects of thermal motions, the step ED profile in Eq. S1 was convoluted with a Gaussian of 2.0 Å width to yield the final gA ED profile shown in Fig. S8. Parameters for the gA dimer are given in Table S6.

Lateral structure. The cylindrical protein domains were assumed to be randomly dispersed within the plane of a lipid bilayer vesicle. The number of domains was calculated from the total surface area of the vesicle, area per lipid, gA concentration, and the effective cross-sectional area a_{cyl} of the gA domain (Table S6). Domains were placed using a random sequential adsorption algorithm, in which trial domain centers were generated randomly and then tested against all previously placed centers for domain overlap; if any overlap existed, the trial domain center was rejected. Fig. S8 shows a representative MC snapshot of protein domains embedded in a vesicle.

Monte Carlo sampling and calculation of SAXS curves. After placing the domains within the vesicle object, random points were generated within radial segments of 0.5 Å width in both the domain and surround regions, with the number of points in a segment being proportional to the magnitude of the ED contrast of that segment with water, and the sign of each point being equal to the sign of that segment's contrast with the water (as given by the ED profiles). Typically, 2×10^3 points were generated per vesicle object. An ED contrast-weighted pair-distance distribution function $P(r)$ was then generated for the vesicle from the combined set of randomly generated points, by calculating all unique pair

distances between points of the same contrast sign (+/+ or –/–) and opposite contrast sign (+/–) and binning them into separate histograms, i.e. $P^{++}(r)$, $P^{--}(r)$, and $P^{+-}(r)$, with $P(r) = P^{++}(r) + P^{--}(r) - P^{+-}(r)$ [15]. This process was repeated for typically 2×10^4 vesicle objects with different randomly placed domains, and the $P(r)$ histograms from the individual vesicles were summed to generate an ensemble-averaged distribution $\bar{P}(r)$. The ensemble-averaged scattering intensity was then calculated as the Fourier transform of $\bar{P}(r)$ [13]:

$$\bar{I}(q) = 4\pi \int_0^\infty \bar{P}(r) \frac{\sin qr}{qr} dr. \qquad (S2)$$

S.4.3. Results

We performed three sets of simulations to isolate the effect of three variables: (1) increasing the concentration of gA transmembrane dimers in the bilayer; (2) increasing the extent of lateral gA aggregation at fixed gA concentration (protein:lipid 1:40); and (3) increasing the extent of perturbation within the first shell of lipids surrounding the gA transmembrane dimer at fixed gA concentration (protein:lipid 1:40).

Effect of increasing gA concentration. Fig. S10 reveals a dramatic liftoff at the first minimum of the simulated SAXS data (q ~ 0.28 Å^{-1}) with increasing concentration of gA transmembrane dimers. This effect arises from lateral ED contrast between the protein domain and the bilayer's hydrocarbon region at short length scales corresponding to the size of the protein domain. Excess scattering at length scales corresponding to domain sizes of tens of nanometers has been observed previously in the context of lipid phase separation in SANS experiments [14]. In that case, the lateral contrast was between an ordered (Lo) phase enriched in chain perdeuterated lipids and a disordered (Ld) phase enriched in protiated lipids [14]. A theoretical treatment of scattering from laterally heterogeneous vesicles predicts that the excess scattering intensity arising from domain/surround contrast will shift to higher q (i.e., smaller real-space distances) with decreasing domain size, and eventually migrate into the minima between scattering lobes, resulting in liftoff [13].

Effect of increasing gA lateral association. The effect of in-plane gA aggregation is shown in Fig. S11. Lateral association of gA into multimers effectively increases the domain size, which shifts the excess scattering toward lower q (i.e., larger real-space distances). The result is a *decrease* in liftoff at q ~ 0.28 Å^{-1} and an *increase* in liftoff at q ~ 0.05 Å^{-1} (far left portion of the figure) with increasing oligomerization state.

Effect of increasing bilayer perturbation. It has been reported that gA causes local thinning of the bilayer for some types of lipids [16, 17]. We investigated the effect of local perturbation by using a different ED profile corresponding to a different area per lipid for the first shell of ~ 14 lipids surrounding the gA transmembrane dimer. Fig. S12 shows the effect of the extent of this perturbation on the simulated SAXS data. Decreasing the thickness (i.e., increasing the area per lipid) of the first shell results in a slight decrease in intensity at the minimum between the first and second scattering lobes, and a slight shift of the minimum to higher q. These effects are subtler than those related to increasing gA concentration or oligomerization state, and might easily be obscured by experimental noise.

S.4.4. Conclusions

The similarity between the simulated data in Fig. S10 and the experimental SAXS data presented in the main text is striking, and strongly suggests that gA was successfully incorporated into the asymmetric vesicles. To our knowledge, ours is the first reported observation of this scattering feature in SAXS data from proteoliposomes. Moreover, because lateral association of gA showed the opposite effect in MC simulations (i.e., a rapid decrease in liftoff with increasing oligomerization, Fig. S11), gA must be predominantly unaggregated in the asymmetric vesicles. The experimental SAXS data from both symmetric and isotopically asymmetric vesicles containing gA do not show a significant change in the position of the first minimum, however conclusions about the extent of perturbation of the POPC bilayer by gA cannot be made due to the relatively poor signal-to-noise of the experimental data. Caution is also warranted due to the coarse-grained nature of the MC simulations as well as the simplifying assumptions that were used (e.g., randomly dispersed cylindrical protein domains). Finer details of the molecular shapes that are not captured by this simple model undoubtedly contribute to the coherent scattering at higher q, and indeed there is a greater discrepancy between experimental and simulated data beyond the second scattering lobe.

References:

1. Chodera, J.D., *A Simple Method for Automated Equilibration Detection in Molecular Simulations.* J Chem Theory Comput, 2016. **12**(4): p. 1799-805.
2. Doktorova, M., et al., *A new computational method for membrane compressibility: Bilayer mechanical thickness revisited.* Biophysical Journal, 2019. **116**(3): p. 487-502.
3. Johner, N., D. Harries, and G. Khelashvili, *Implementation of a methodology for determining elastic properties of lipid assemblies from molecular dynamics simulations.* BMC Bioinformatics, 2016. **17**: p. 161.
4. Johner, N., D. Harries, and G. Khelashvili, *Erratum to: Implementation of a methodology for determining elastic properties of lipid assemblies from molecular dynamics simulations.* BMC Bioinformatics, 2016. **17**(1): p. 236.
5. Doktorova, M., D. Harries, and G. Khelashvili, *Determination of bending rigidity and tilt modulus of lipid membranes from real-space fluctuation analysis of molecular dynamics simulations.* Phys Chem Chem Phys, 2017. **19**(25): p. 16806-16818.
6. Kucerka, N., M.P. Nieh, and J. Katsaras, *Fluid phase lipid areas and bilayer thicknesses of commonly used phosphatidylcholines as a function of temperature.* Biochim Biophys Acta, 2011. **1808**(11): p. 2761-71.
7. Doktorova, M., et al., *Preparation of asymmetric phospholipid vesicles for use as cell membrane models.* Nat Protoc, 2018. **13**(9): p. 2086-2101.
8. Guixa-Gonzalez, R., et al., *MEMBPLUGIN: studying membrane complexity in VMD.* Bioinformatics, 2014. **30**(10): p. 1478-80.

9. Mondal, S., et al., *Quantitative modeling of membrane deformations by multihelical membrane proteins: application to G-protein coupled receptors.* Biophys J, 2011. **101**(9): p. 2092-101.
10. Doktorova, M., et al., *Cholesterol Promotes Protein Binding by Affecting Membrane Electrostatics and Solvation Properties.* Biophys J, 2017. **113**(9): p. 2004-2015.
11. Heberle, F.A., et al., *Model-based approaches for the determination of lipid bilayer structure from small-angle neutron and X-ray scattering data.* Eur Biophys J, 2012. **41**(10): p. 875-90.
12. Kucerka, N., et al., *Structural Significance of Lipid Diversity as Studied by Small Angle Neutron and X-ray Scattering.* Membranes (Basel), 2015. **5**(3): p. 454-72.
13. Heberle, F.A., V.N. Anghel, and J. Katsaras, *Scattering from phase-separated vesicles. I. An analytical form factor for multiple static domains.* Journal of Applied Crystallography, 2015. **48**(5): p. 1391-1404.
14. Heberle, F.A., et al., *Bilayer thickness mismatch controls domain size in model membranes.* J Am Chem Soc, 2013. **135**(18): p. 6853-9.
15. Henderson, S.J., *Monte Carlo modeling of small-angle scattering data from non-interacting homogeneous and heterogeneous particles in solution.* Biophysical Journal, 1996. **70**(4): p. 1618-1627.
16. Harroun, T.A., et al., *Experimental evidence for hydrophobic matching and membrane-mediated interactions in lipid bilayers containing gramicidin.* Biophys J, 1999. **76**(2): p. 937-45.
17. Kim, T., et al., *Influence of hydrophobic mismatch on structures and dynamics of gramicidin a and lipid bilayers.* Biophys J, 2012. **102**(7): p. 1551-60.